SUPPLEMENTARY INFORMATION

Novel pyrrolo[3,2-*d*]pyrimidine compounds target mitochondrial and cytosolic one-carbon metabolism with broad-spectrum antitumor efficacy

Aamod S. Dekhne[1], Khushbu Shah[2], Gregory S. Ducker[3], Jade M. Katinas[4], Jennifer Wong-Roushar[4], Md. Junayed Nayeen[2], Arpit Doshi[2], Changwen Ning[5], Xun Bao[1], Josephine Frühauf[1], Jenney Liu[6], Adrianne Wallace-Povirk[1], Carrie O'Connor[1], Sijana H. Dzinic[1], Kathryn White[1], Juiwanna Kushner[1], Seongho Kim[1], Maik Hüttemann[6], Lisa Polin[1], Joshua D. Rabinowitz[3], Jing Li[1], Zhanjun Hou[1], Charles E. Dann III[4a], Aleem Gangjee[2a], and Larry H. Matherly[1a]

[1]Department of Oncology, Wayne State University School of Medicine, and the Barbara Ann Karmanos Cancer Institute, Detroit, MI 48201
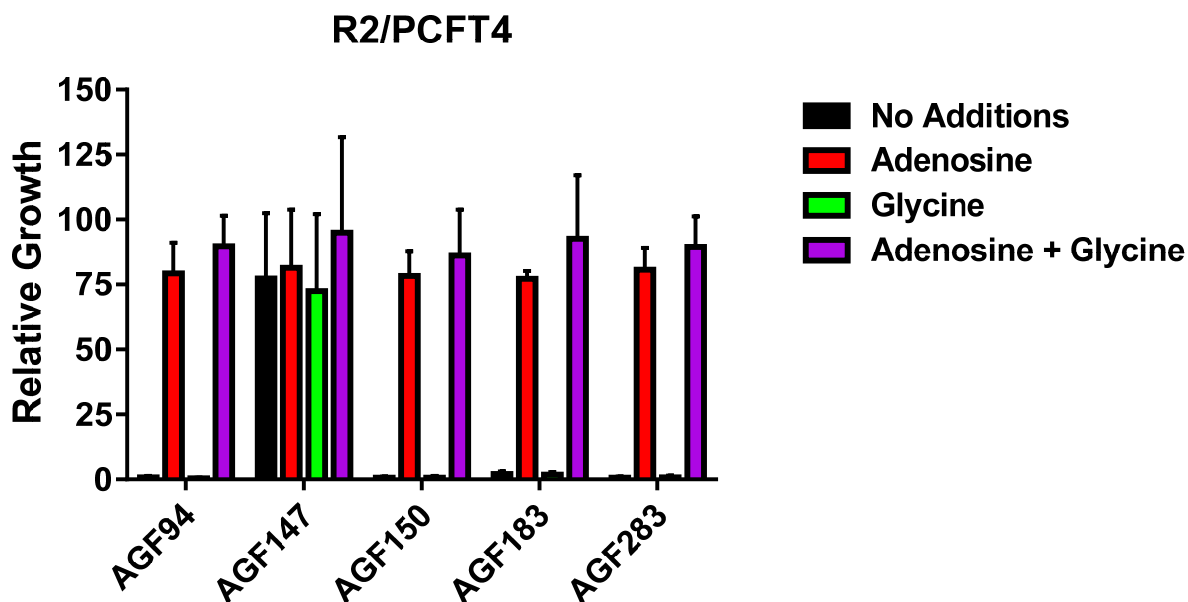
[2]Division of Medicinal Chemistry, Graduate School of Pharmaceutical Sciences, Duquesne University, Pittsburgh, PA 15282

[3]Department of Chemistry/Lewis-Sigler Institute for Integrative Genomics, Princeton University, Princeton NJ 08544

[4]Department of Chemistry, Indiana University, Bloomington, IN 47405

[5]Biochemistry and Molecular Biology, Jilin University, Changchun, Jilin Province, China

[6]Center for Molecular Medicine and Genetics, Wayne State University School of Medicine, Detroit, MI 48201

R2/PCFT4

Legend:
- No Additions (black)
- Adenosine (red)
- Glycine (green)
- Adenosine + Glycine (purple)

Y-axis: Relative Growth
X-axis categories: AGF94, AGF147, AGF150, AGF183, AGF283

Figure S1. *In vitro* **antiproliferative activity and identification of targeted pathways and enzymes by previously reported AICARFTase and GARFTase inhibitors (1-5).** Results are shown for relative proliferation of R2/PCFT4 Chinese hamster ovary (CHO) cells treated with inhibitor (1 μM) alone, or in the presence of adenosine (60 μM) and/or glycine (130 μM). The experiments were performed in complete folate-free RPMI1640, supplemented with 25 nM leucovorin without added glycine (see **Materials and Methods**). The results are presented as mean values ± standard deviations for at least three biological replicates, with growth of cells treated with inhibitor ± metabolite normalized to the growth of cells treated with vehicle (i.e., DMSO) ± metabolite.
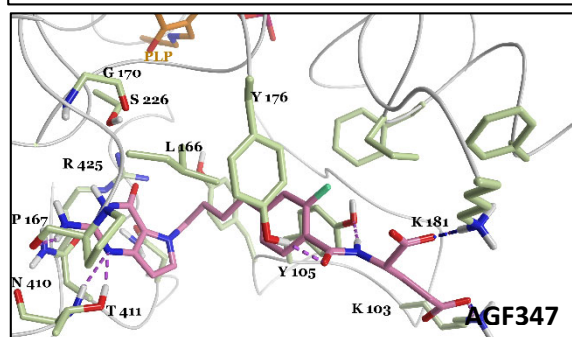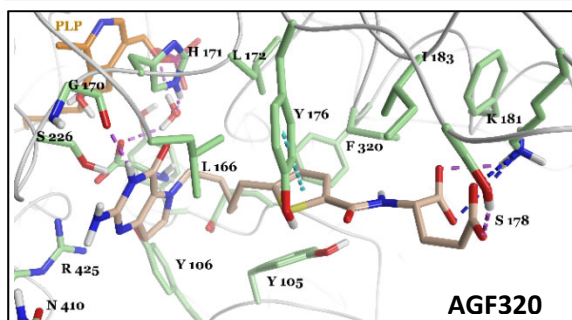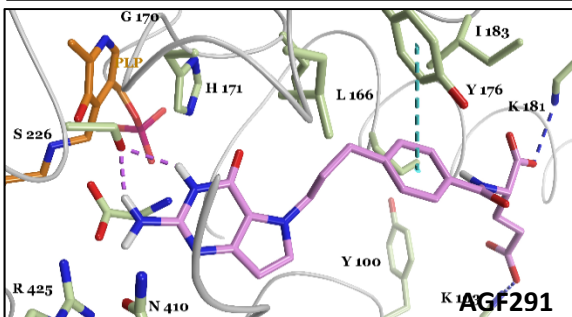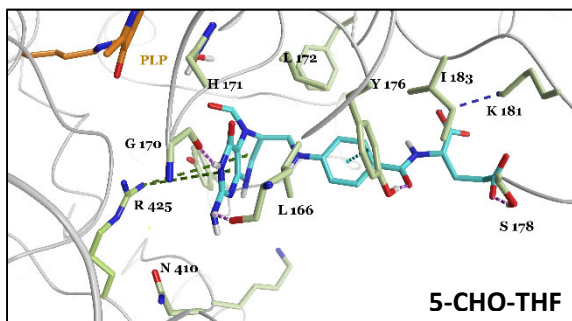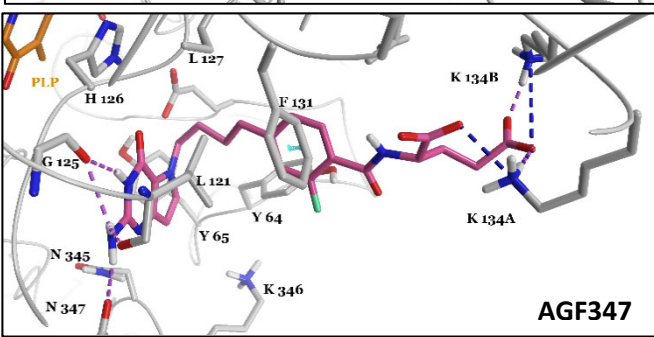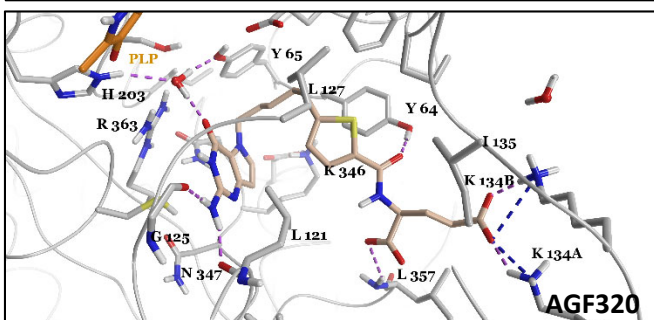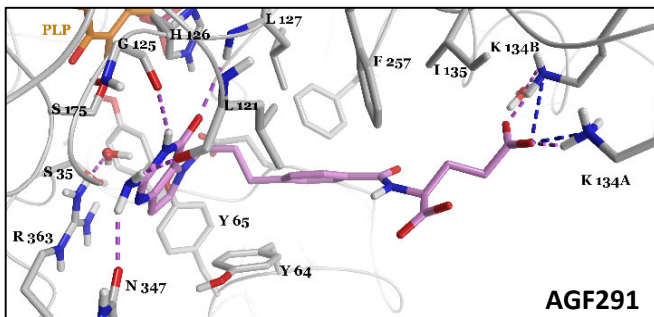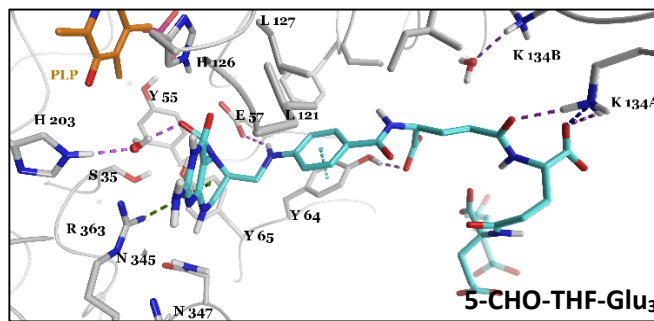
Figure S2. Docked poses of 5-formyl tetrahydrofolate (5-CHO-THF), AGF291, AGF320, and AGF347 in the human dimeric SHMT2 crystal structure (PDB: 5V7I) (6); crystal structure of 5-formyl THF triglutamate (5-CHO-THF-Glu$_3$) in rabbit SHMT1 (PDB: 1L53) (7) and docked poses of AGF291, AGF320, and AGF347 in the rabbit SHMT1 structure. Molecular modeling was performed using the induced fit docking protocol of Maestro (8,9). The docking scores for all the proposed analogs in SHMT2 and SHMT1 are in **Supplementary Table S1**. With SHMT2, the pyrrolo[3,2-*d*]pyrimidine scaffold of **AGF347** (best SHMT2 docking score of the series (**Table S1**)), occupies the pocket lined by Leu166, Asn410, Gly170, and Arg425. The 2-NH$_2$ group makes a hydrogen bond (faded plum color) with the backbone CO of Pro167, and N1 forms a hydrogen bond with the Thr411 hydroxyl group and backbone NH. The four carbon alkyl chain linker orients in a similar way as the linker at the C6 position of 5-CHO-THF in the SHMT1 crystal structure. The 2-fluorophenyl ring is sandwiched between Tyr176 and Tyr105. The 2-fluoro substitution makes a steric clash with the carbonyl oxygen of the amide group, forcing the amide group perpendicular to the phenyl ring, which further forces the hydrogen bond with the Tyr176 and Tyr105 hydroxyl groups. The α- and γ-COOH groups of the L-glutamyl side chain form a salt bridge (blue color dotted line) with Lys181 and Lys103. These ionic interactions are preserved for **AGF291** and **AGF320** in SHMT2, and with the aromatic side chains (phenyl and thienoyl, respectively), resulting in a pi-pi interaction (cyan color dotted line) with Tyr176. **AGF320** shows the highest docking score among all the proposed analogs for SHMT1 (**Table S1**). The pyrrolo[3,2-*d*]pyrimidine scaffold for **AGF320** in SHMT1 sits in the pocket occupied by Leu121, Leu127, Gly125, His203, Arg363, Lys346, and Asn347. The 2-NH$_2$ group makes hydrogen bonds (faded plum) with the backbone CO of Leu121 and Gly125. The 4-oxo makes a water-mediated hydrogen bond with Tyr65 and His203. The α-COOH makes a hydrogen bond with the backbone of Leu357 and the γ-COOH forms a salt-bridge (blue dotted line) with Lys134B.
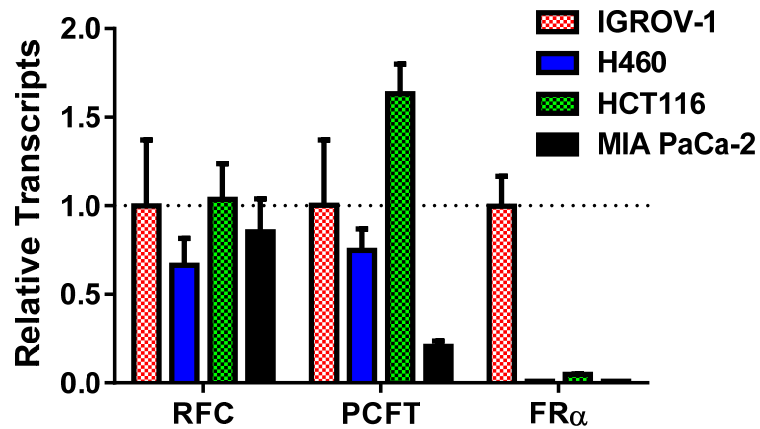
Figure S3. Folate transporter transcript expression of human tumor cell lines by RT-PCR.
Transcript levels for the reduced folate carrier (RFC), proton-coupled folate transporter (PCFT) and folate receptor alpha (FRα) in H460, HCT116, MIA PaCa-2, and IGROV-1 cells were measured by real-time RT-PCR with results normalized to those of β-actin and GAPDH. Methods are described in **Materials and Methods**. The results represent three experimental replicates with individual transporter expression within each replicate normalized to the average of the corresponding transporter expression across all IGROV-1 replicates. The results represent mean values +/- standard deviations. Although H460, HCT116 and MIA PaCa-2 cells all express abundant RFC and PCFT, FRα expression is negligible in these cells.
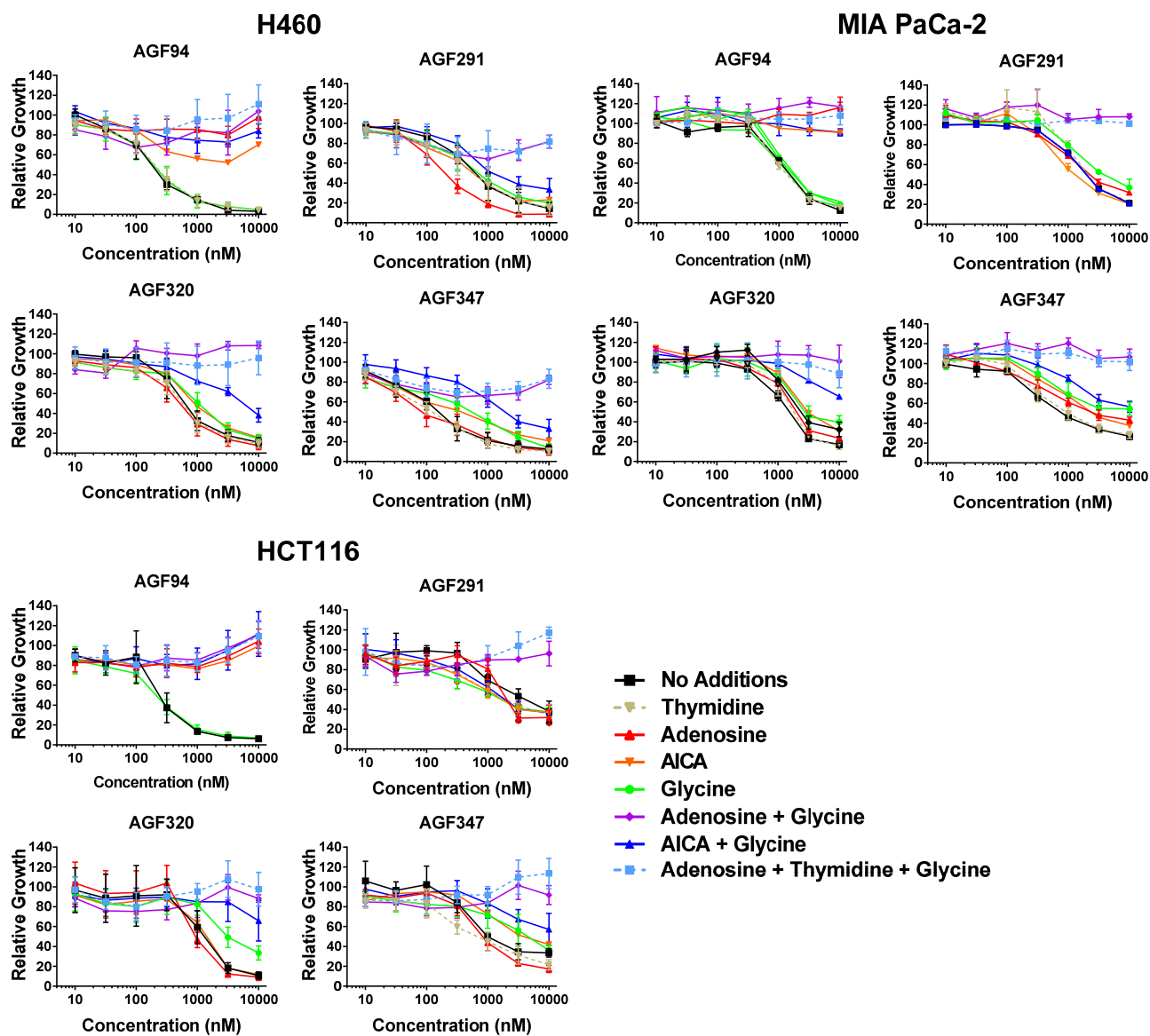
Figure S4. *In vitro* antitumor efficacy and identification of targeted pathways and enzymes by AGF94 and novel 5-substituted pyrrolo[3,2-*d*]pyrimidine benzoyl and thienoyl analogs in H460, MIA PaCa-2, and HCT116 tumor cells. Dose-response curves are shown for **AGF94**, an established β-glycinamide ribonucleotide formyltransferase (GARFTase) inhibitor (3) and the 5-substituted pyrrolo[3,2-*d*]pyrimidine compounds **AGF291**, **AGF320**, and **AGF347** without additions, or in the presence of adenosine (60 μM), 5-aminoimidazole-4-carboxamide (AICA) (320 μM), thymidine (10 μM) and/or glycine (130 μM). The experiments were performed in complete folate-free RPMI1640, supplemented with 25 nM leucovorin without added glycine (see **Materials and Methods**). The results are presented as mean values ± standard deviations from at least three biological replicates, with growth of cells treated with inhibitor ± metabolite normalized to the growth of cells treated with vehicle (i.e., DMSO) ± metabolite.
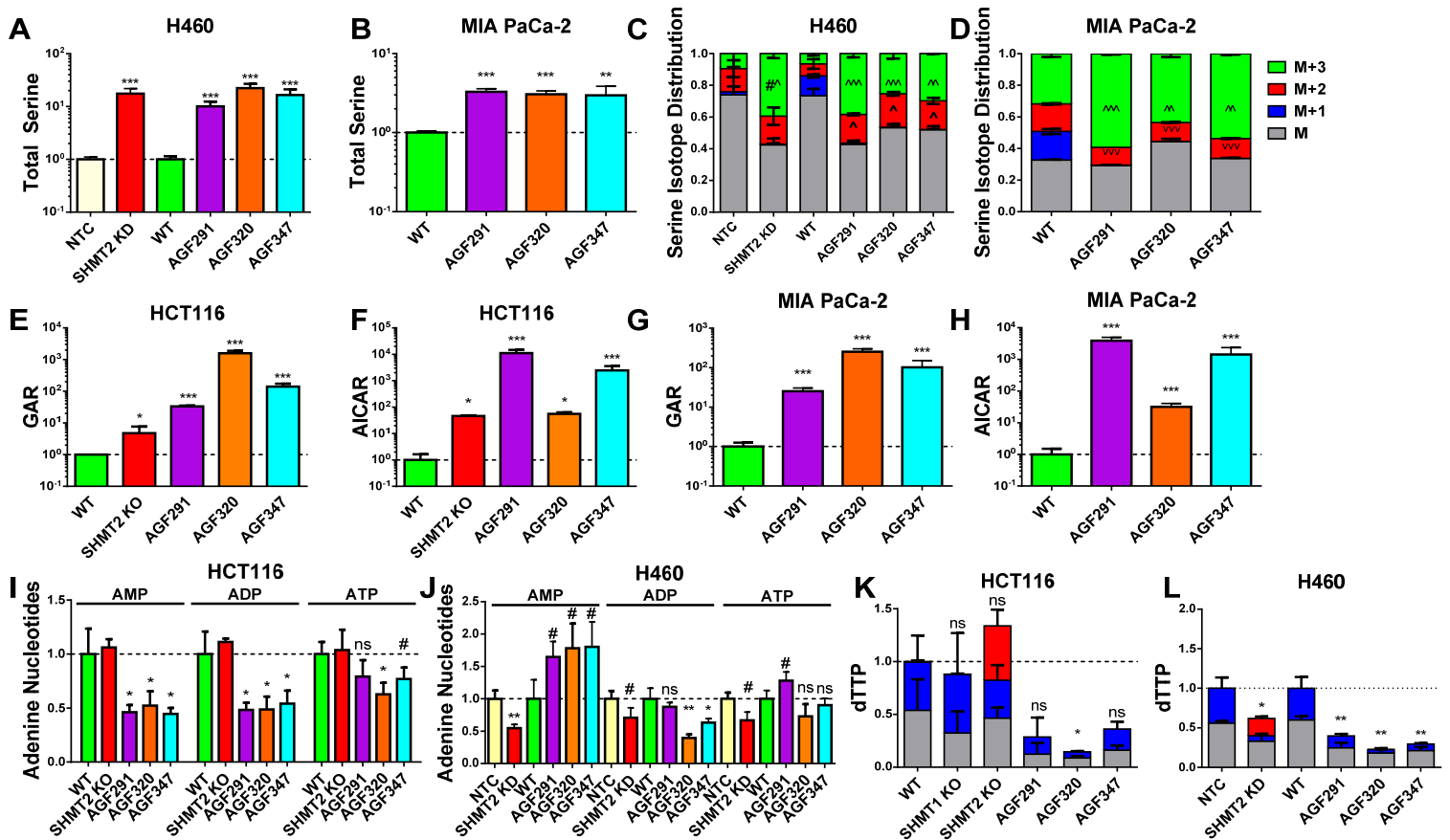
Figure S5. Targeted metabolomics analysis to identify intracellular enzyme targets of AGF291, AGF320, and AGF347 in HCT116, H460, and MIA PaCa-2 cells. Cells were incubated with the inhibitors or vehicle for 16 hours in glycine-replete, folate-free complete RPMI 1640, supplemented with 25 nM leucovorin (including unlabeled serine). The media was replaced with media (including inhibitor or vehicle) and 250 µM [2,3,3-^{2}H]serine for another 24 hours, after which metabolites were extracted for LC-MS analysis. **Top row:** Total serine pools and serine isotope distributions for H460 (**A and C, respectively**) and MIA PaCa-2 (**B and D, respectively**) cells are shown. **Middle row:** GAR and AICAR accumulations in HCT116 (**E and F, respectively**) and MIA PaCa-2 (**G and H, respectively**) cells are shown. **Bottom row:** Total adenine nucleotide pools and total dTTP pools including dTTP isotope distributions for HCT116 (**I and K, respectively**) and MIA PaCa-2 (**J and L, respectively**) cells are shown. Results reflect three technical replicates. #, p < 0.10; *, p < 0.05; **, p < 0.01; ***, p < 0.001; ^ or ˅ are used in place of * to specify a significant increase or decrease respectively; ns = not significant. Statistical comparisons were made between inhibitor-treated/knockout (KO)/knockdown (KD) samples and DMSO-treated wild-type (WT) or non-targeted control (NTC) samples, as appropriate.
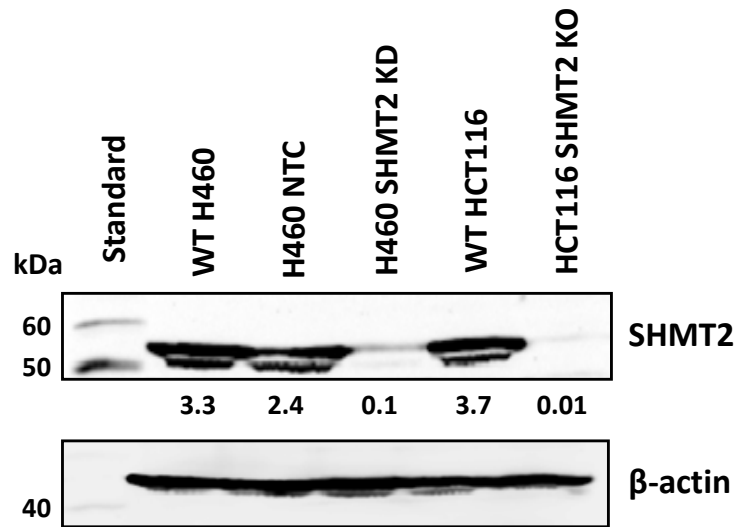
Figure S6. Western blot confirming H460 SHMT2 knockdown and HCT116 SHMT2 knockout. Whole-cell lysates of wild-type (WT), non-targeted control shRNA-transduced (NTC), and clonal SHMT2 knockdown (SHMT2 KD) H460 cells, along with HCT116 WT and SHMT2 CRISPR/Cas9 knockout (KO) cells were resolved on a 10% polyacrylamide gel with SDS and probed with monoclonal rabbit anti-SHMT2 antibody (#12762; Cell Signaling Technology, Danvers, MA). The blot was stripped and reprobed with mouse anti-β-actin antibody (Sigma-Aldrich) as a loading control. Experimental details are described in **Materials and Methods**. The blots were scanned with an Odyssey infrared imaging system (LICOR Biosciences). Densitometry analysis (values shown are SHMT2 band intensities normalized to β-actin band intensities) revealed SHMT2 protein expression of H460 SHMT2 KD cells to be 5.3% of that of H460 NTC cells, and HCT116 SHMT2 KO expression to be <1% of that of HCT116 WT cells.
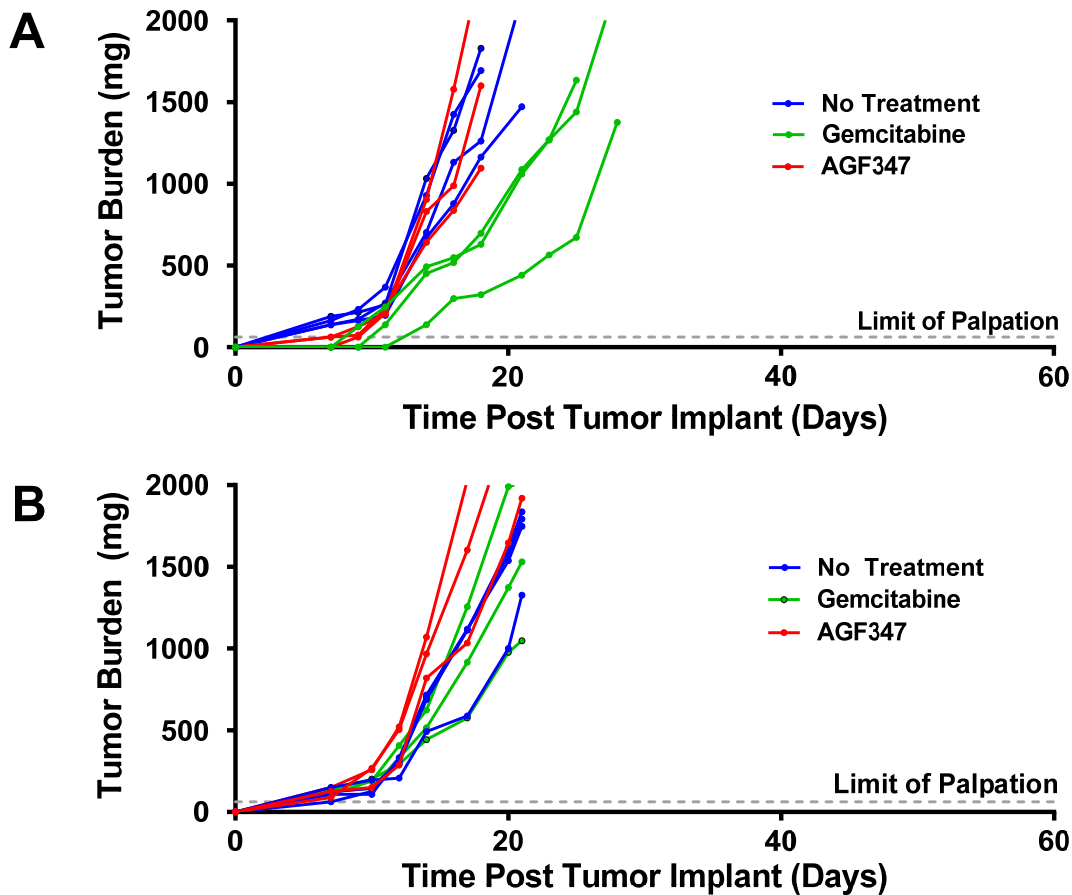
Figure S7. *In vivo* efficacies of AGF347 and GEM toward MIA PaCa-2 xenografts in mice fed a standard diet. **A:** Female NCr SCID mice (11 weeks old 20.2 g average body weight) were implanted bilaterally with human MIA PaCa-2 pancreatic cancer xenograft fragments. Treatment was initiated on day 1 following SC tumor implantation. The mice were dosed as follows: **AGF347**, Q2dx8 at 15 mg/kg/injection, total dose 120 mg/kg; and GEM, Q4dx4 at 120 mg/kg/IV injection, total dose 480 mg/kg. Results are shown for individual mice. **B:** Female ICR SCID mice (10 weeks old; 19 g average body weight) were implanted bilaterally with human MIA PaCa-2 PaC tumors. On day 7 following subcutaneous implantation, the mice were dosed as for (**A**).
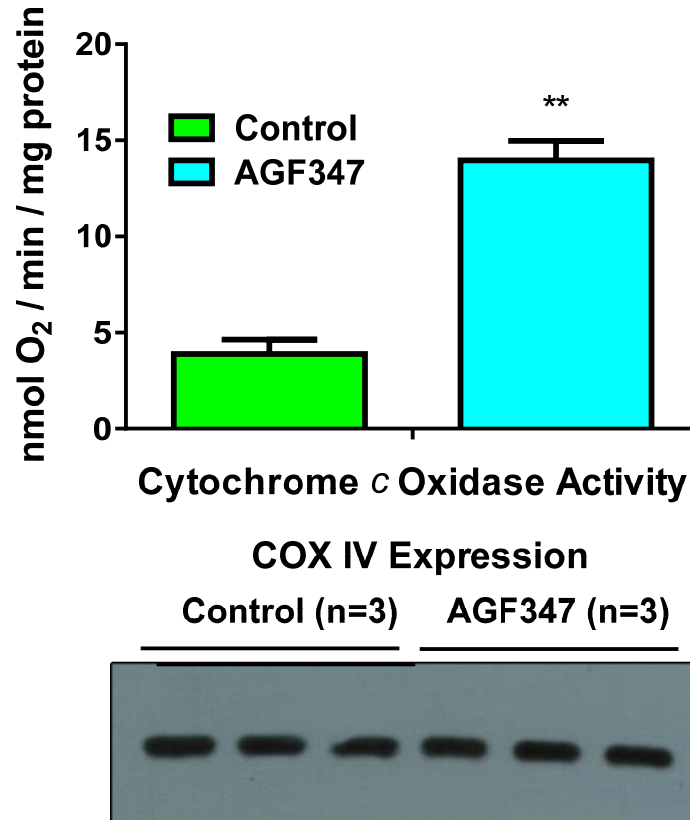
Figure S8. Cytochrome *c* oxidase assay of control and AGF347-treated MIA PaCa-2 xenografts. Tumor samples harvested from the MIA PaCa-2 tumor xenograft metabolomics arm were assayed for cytochrome *c* oxidase activity. After the 6th injection of **AGF347**, both vehicle-treated and **AGF347**-treated mice were euthanized and tumors harvested and snap-frozen in liquid nitrogen. Tumor samples (from three separate **AGF347**-treated and three separate control mice) were solubilized in HEPES solubilization buffer. Equal amounts of protein from each sample (confirmed by Western Blot, inset) were treated with bovine heart cytochrome *c* and oxygen consumption was measured. Details are provided in Supporting Information Methods.

Table S1. Docking scores of pyrrolo[3,2-*d*]pyrimidine compounds for intracellular drug targets (kcal/mol)		
Compound	SHMT2	SHMT1
AGF291	-7.69	-10.45
AGF299	-7.42	-7.48
AGF300	-7.58	-7.17
AGF318	-6.43	-7.03
AGF320	-8.32	-11.14
AGF331	-6.93	-7.19
AGF347	-10.06	-8.90
AGF355	-6.55	-6.45
Molecular modeling was performed for all analogs with the structure of human SHMT2 (PDB: 5V7I) (6) and rabbit SHMT1 (PDB: 1LS3) (7), using the induced fit docking protocol of Maestro (8,9). Further details are described in **Materials and Methods.**		

Table S2. Antitumor Efficacy Evaluation of AGF347 and Gemcitabine Against Human MIA PaCa-2 Pancreatic Adenocarcinoma xenografts in Female NCR SCID Mice

Early Stage

Treatment	Route	Schedule	Total Dosage (mg/kg)	Mean Body Weight Loss (g/mouse) at Nadir (day)	Percent Body Weight. Loss	Median Tumor Burden in mg on Day 16 (range)	T/C (%)	Tumor Free on Day 136	Time to 1000 mg in Days (range)	Tumor Growth Delay (days)	Log Cell Kill
No Treatment	—	—	—	+0.8 (d16)	+3.9	1189 (601 – 1711)	—	0/5	15 (12.5 – 20)	—	—
Gemcitabine	IV	Q4dx4 Start day1	480	-1.4 (d3)	-6.9	420 (284 – 552)	35	0/5	21 (19 – 24)	6	1.1
AGF347	IV	Q2dx8 Start day1	120	-0.2 (d17)	-1.0	0 (0 – 276)	0	1/5	54 (21 – 77)*	39*	>5.0*

Late Stage

Treatment	Route	Schedule	Total Dosage (mg/kg)	Mean Body Weight. Loss in g/mouse at Nadir (day)	Percent Body Weight Loss	Median Tumor Burden in mg on Day 21 (range)	PR (CR)	T/C %	Tumor Free on Day 69	Time to 1000 mg in Days (range)	Tumor Growth Delay (days)	Log Cell Kill
No Treatment	—	—	—	-0.4 (d8)	-2.0	1736 (1117-2046)	0	—	0/5	17 (15-20)	—	—
Gemcitabine	IV	Q4dx4 Start d7	480	-1.0 (d20)	-5.1	524 (247-1045)	0	30	0/5	28 (23-42)	11	1.9
AGF347	IV	Q2dx8 Start d7	120	-0.2 (d21)	-1.0	733 (373-1835)	2 (1)	42	0/5	24 (15-69)	7	1.2

In vivo efficacies of **AGF347** and gemcitabine (GEM) toward the MIA PaCa-2 xenografts. Female NCr SCID mice (11 weeks old; 20.2 g average body weight – early stage, 10 weeks old; 19 g average body weight – late stage) were implanted bilaterally with human MIA PaCa-2 tumor fragments on day 0. For the efficacy trial, starting 16 days before subcutaneous (SC) tumor implant, the mice were maintained on a folate-deficient diet to ensure that serum folate levels would approximate those of humans (1-5). The mice were unselectively distributed to the treatment and control arms (5 mice per group). Beginning on day one (early stage) or day seven (late stage) following SC implantation, the mice were dosed intravenously (IV) as follows: **AGF347**, Q2dx8 at 15 mg/kg/injection, total dose 120 mg/kg; and GEM, Q4dx4 at 120 mg/kg/injection, total dose 480 mg/kg. The mice were weighed and their health conditions assessed daily; tumors were measured by caliper two-to-three times weekly. Mice were sacrificed when the cumulative tumor burden reached 5-10% of body weight (1-2 g). Tumor volumes were estimated from two-dimensional caliper measurements, where tumor mass (in mg) = (a x b^2)/2, and a and b are the tumor length and width in mm, respectively. The tumor masses from both flanks of each mouse were added together, and the total mass per mouse was used for calculations of antitumor activity. Quantitative end-points include: (i) tumor growth delay [T-C, where T is the median time in days required for the treatment group tumors to reach a predetermined size (e.g., 1000 mg), and C is the median time in days for the control group tumors to reach the same size; tumor-free survivors are excluded from these calculations]; and (ii) gross log$_{10}$ cell kill (LCK) [determined by the formula, LCK = (T-C; tumor growth delay in days)/3.32 x Td (tumor doubling time in days determined by growth plot)]. Further analysis included determinations of T/C values (in percent) on all days of tumor measurement using the median total tumor burden for treatment (T) and control (C) groups. The reported %T/C value for this study corresponds to the first measurement taken post last treatment [day 16 (early stage) or day 21 (late stage), when control tumors were still in exponential growth phase, i.e., 500-1250 mg]. The median value of each group was determined including zeros. The %T/C value is the inverse of tumor growth inhibition (TGI). Mouse body weight, percent body weight loss and host recovery time (time in days for mice to regain starting weight from weight loss nadir; data not shown) were used, along with daily health monitoring, to gauge drug effects and potential toxicity, and to determine the optimal highest non-toxic total dose schedules. Definitions: partial remission (PR), treatment-induced tumor burden nadir < 50% of peak tumor burden after tumor engraftment (i.e. tumor burden > 200 mg); and complete response (CR), treatment-induced tumor burden nadir = 0 mg after tumor engraftment.*These measurements omit the single tumor-free mouse in this group.

References

1. Golani, L. K., Wallace-Povirk, A., Deis, S. M., Wong, J. E., Ke, J., Gu, X., Raghavan, S., Wilson, M. R., Li, X., Polin, L., de Waal, P. W., White, K., Kushner, J., O'Connor, C., Hou, Z., Xu, H. E., Melcher, K., Dann, C. E., Matherly, L. H., and Gangjee, A. (2016) Tumor targeting with novel 6-substituted pyrrolo[2,3-d]pyrimidine antifolates with heteroatom bridge substitutions via cellular uptake by folate receptor α and the proton-coupled folate transporter and inhibition of de novo purine nucleotide biosynthesis. *J Med Chem* **59**, 7856-7876

2. Ravindra, M. P., Wilson, M. R., Tong, N., O'Connor, C., Karim, M. A., Polin, L., Wallace-Povirk, A., White, K., Kushner, J., Hou, Z., Matherly, L. H., and Gangjee, A. (2018) Fluorinated substituted pyrrolo[2,3-d]pyrimidine antifolates with tumor-targeting via cellular uptake by folate receptor α and the proton-coupled folate transporter and inhibition of de novo purine nucleotide biosynthesis. *J Med Chem*

3. Wang, L., Desmoulin, S. K., Cherian, C., Polin, L., White, K., Kushner, J., Fulterer, A., Chang, M.-H., Mitchell, S., Stout, M., Romero, M. F., Hou, Z., Matherly, L. H., and Gangjee, A. (2011) Synthesis, biological and antitumor activity of a highly potent 6-substituted pyrrolo[2,3-d]pyrimidine thienoyl antifolate inhibitor with proton-coupled folate transporter and folate receptor selectivity over the reduced folate carrier that inhibits β-glycinamide ribonucleotide formyltransferase. *J Med Chem* **54**, 7150-7164

4. Wang, L., Wallace, A., Raghavan, S., Deis, S. M., Wilson, M. R., Yang, S., Polin, L., White, K., Kushner, J., Orr, S., George, C., O'Connor, C., Hou, Z., Mitchell-Ryan, S., Dann, C. E., Matherly, L. H., and Gangjee, A. (2015) 6-Substituted pyrrolo[2,3-d]pyrimidine thienoyl regioisomers as targeted antifolates for folate receptor α and the proton-coupled folate transporter in human tumors. *J Med Chem* **58**, 6938-6959

5. Wang, Y., Cherian, C., Orr, S., Mitchell-Ryan, S., Hou, Z., Raghavan, S., Matherly, L. H., and Gangjee, A. (2013) Tumor-targeting with novel non-benzoyl 6-substituted straight chain pyrrolo[2,3-d]pyrimidine antifolates via cellular uptake by folate receptor α and inhibition of de novo purine nucleotide biosynthesis. *J of Med Chem* **56**, 10.1021/jm401139z

6. Ducker, G. S., Ghergurovich, J. M., Mainolfi, N., Suri, V., Jeong, S. K., Hsin-Jung Li, S., Friedman, A., Manfredi, M. G., Gitai, Z., Kim, H., and Rabinowitz, J. D. (2017) Human SHMT inhibitors reveal defective glycine import as a targetable metabolic vulnerability of diffuse large B-cell lymphoma. *Proc Natl Acad Sci U S A* **114**, 11404-11409

7. Fu, T. F., Scarsdale, J. N., Kazanina, G., Schirch, V., and Wright, H. T. (2003) Location of the pteroylpolyglutamate-binding site on rabbit cytosolic serine hydroxymethyltransferase. *J Biol Chem* **278**, 2645-2653

8. Fu, T. F., Rife, J. P., and Schirch, V. (2001) The role of serine hydroxymethyltransferase isozymes in one-carbon metabolism in MCF-7 cells as determined by (13)C NMR. *Arch Biochem Biophys* **393**, 42-50

9. Jain, M., Nilsson, R., Sharma, S., Madhusudhan, N., Kitami, T., Souza, A. L., Kafri, R., Kirschner, M. W., Clish, C. B., and Mootha, V. K. (2012) Metabolite profiling identifies a key role for glycine in rapid cancer cell proliferation. *Science (New York, N.Y.)* **336**, 1040-1044